A physiologically motivated sparse, compact, and smooth (SCS) approach to EEG source localization

Cheng Cao, Zeynep Akalin Acar, Kenneth Kreutz-Delgado, Scott Makeig

Abstract— **Here, we introduce a novel approach to the EEG inverse problem based on the assumption that principal cortical sources of multi-channel EEG recordings may be assumed to be spatially sparse, compact, and smooth (SCS). To enforce these characteristics of solutions to the EEG inverse problem, we propose a correlation-variance model which factors a cortical source space covariance matrix into the multiplication of a pre-given correlation coefficient matrix and the square root of the diagonal variance matrix learned from the data under a Bayesian learning framework. We tested the SCS method using simulated EEG data with various SNR and applied it to a real ECOG data set. We compare the results of SCS to those of an established SBL algorithm.**

I. Introduction

Electroencephalography(EEG) and its magnetic equivalent, magnetoencephalography (MEG) measure voltage potential or electromagnetic field generated by current sources located within the brain using multiple sensors located on or near the scalp. Compared to the long-time (more than 5-s) delay between the firing of neurons and the peak of BOLD signal from functional magnetic resonance imaging (fMRI), EEG and MEG have much higher temporal resolution. However, accurately determining the spatial locations of the current sources is extremely difficult since the mapping from source activity configuration to sensor measurement is many to one, and hence underdetermined. Thus EEG source localization is an ill-posed inverse problem.

To remedy the ill-posed nature of the EEG source localization inverse problem, two types of solution conditions are commonly enforced or encouraged: (a) smoothness, and (b) sparsity. Minimum Norm Estimates (MNE), LORETA, and other linear regulation-based methods encourage source smoothness ([1],[2],[3]), while Sparse Bayesian Learning (SBL) algorithms encourage source sparsity ([4],[5]). Attempting to enforce these two conditions drives solutions in opposite directions: smoothing tends to keep a large portion of the current dipoles in the source space "active," while sparse learning reduces the activity of most current dipoles to zero, tending to produce a sparse pattern of isolated delta-function like dipole activations. However, in reality, neuronal networks of the brain, and specifically within the cortex, exhibit a quasi 'small world' property in which neurons synchronize mainly with their immediate neighbors through short-distance connections, with relatively few long-range connections that are capable of supporting long-distance field synchrony. Therefore, the current sources contributing to EEG signals should be *both* spatially compact *and* locally smooth, typically taking the form of a compact, but non-point like, cortical source patch comprised of parallel dipolar activations.

Highly overlapping (linearly mixed) far-field scalp projections of spatially distinct, locally synchronous cortical field activities can be separated from recorded EEG scalp data by independent component analysis (ICA) [6]. In practice, ICA returns component source processes whose projections to the scalp are highly compatible with the synchronous or near-synchronous projection of a single compact cortical patch [7]. Further, the more efficient the ICA approach, the more such 'dipolar' sources result from blind source separation of EEG data [8].

II. Bayesian Modeling using General Gaussian Scale Matrix and Arbitrary Covariance Matrix

The EEG/EMG source localization problem is to solve the under-determined linear inverse problem

$$\boldsymbol{p} = \mathbf{G}\boldsymbol{d} + \boldsymbol{n} \tag{1}$$

Eq. (1) models the projection of a source through EEG forward head model at a single time point. Its terms consist of a recorded data vector (at m channels) $\boldsymbol{p}$, a dipolar $m \times n$ gain matrix $\mathbf{G}$ (the 'lead field matrix' relating n dipolar source strengths to the m recorded scalp potentials, $\boldsymbol{n} \gg \boldsymbol{m}$), a vector of dipole source strengths $\boldsymbol{d}$, plus a noise vector $\boldsymbol{n}$. Because the number of sensors is much less than the number of dipoles, there are an infinite number of possible values of $\boldsymbol{d}$ that satisfy (1), even when the noise $\boldsymbol{n}$ is zero. Thus, prior knowledge about the nature of the sources is essential for finding a unique and useful solution of the inverse problem. In a Bayesian framework, as formalized in (2), such knowledge is embedded in the prior distribution P($\boldsymbol{d}$).

$$P(\boldsymbol{d}|\boldsymbol{p}) = P(\boldsymbol{p}|\boldsymbol{d})P(\boldsymbol{d})/P(\boldsymbol{p}) \tag{2}$$

In the case of many approaches, such as minimum l_2-norm approaches, minimum current estimation (MCE), SLORETA, etc., it is often assumed that both the dipole strength vector $\boldsymbol{d}$ and the noise vector $\boldsymbol{n}$ are normally distributed with zero mean and known covariance matrices $\mathbf{\Sigma}_d$ and $\mathbf{\Sigma}_n$. Alternative, sparsity-inducing Bayesian methods learn the form of $P(\boldsymbol{d})$ from the observed data by updating a set of flexible hyperparameters $\boldsymbol{\gamma}$. A specific formalization of this approach may be presented in the generalized framework [3]:

$$P(\boldsymbol{p}|\boldsymbol{d}) \propto \exp\left(-\tfrac{1}{2}(\boldsymbol{p} - \mathbf{G}\boldsymbol{d})^T \Sigma_{\boldsymbol{n}}^{-1}(\boldsymbol{p} - \mathbf{G}\boldsymbol{d})\right) \tag{3}$$

$$\Sigma_{\boldsymbol{d}} = \sum_{i=1}^{d_{\boldsymbol{\gamma}}} \gamma_i \boldsymbol{C}_i \tag{4}$$

The noise covariance matrix $\mathbf{\Sigma}_n$ can be estimated from the data or may be fixed based on prior knowledge. Here, for simplicity we assumed that $\mathbf{\Sigma}_n$ is diagonal, with $\mathbf{\Sigma}_n(i,i) = \varepsilon_i^2$ providing a prior estimate of noise variance at the i-th channel. In (4), $\boldsymbol{\gamma} \triangleq [\gamma_1, \ldots \gamma_{d_{\boldsymbol{\gamma}}}]^T$ is a vector of $d_{\boldsymbol{\gamma}}$ nonnegative hyperparameters. The appropriate covariance $\sum_{\boldsymbol{d}}$ can be estimated by modifying $\boldsymbol{\gamma}$, whose components control the relative contribution of each covariance basis $\boldsymbol{C}_i$.

*Research supported by an ONR BRC project (SM, P.I.), and by The Swartz Foundation (Old Field, NY)

C. Cao, Z, Akalin Acar, S. Makeig are with the Swartz Center of Computational Neuroscience (SCCN), INC, Univ of California San Diego, CA, USA. (email:{cheng, zeynep, scott}@sccn.ucsd).

K. Kreutz-Delgado is with Dept. of Electrical and Computer Engineering, Jacobs School of Engineering, University of California, San Diego, CA, USA. (email: kreutz@ece.ucsd.edu).

The proper hyperparameter $\boldsymbol{\gamma}$ can be estimated by hyperparameter MAP estimation (γ-MAP) [3] which maximizes hyperparameter likelihood $P(\boldsymbol{p}|\boldsymbol{\gamma})$. This is equivalent to minimizing the cost function

$$\boldsymbol{L}(\gamma) = \boldsymbol{p}^T\Sigma_{\boldsymbol{p}}^{-1}\boldsymbol{p} + \log(|\Sigma_{\boldsymbol{p}}|) \quad (5)$$

where

$$\boldsymbol{\Sigma_p}=\mathbf{G}\boldsymbol{\Sigma_d}\mathbf{G}^T+\boldsymbol{\Sigma_n} \quad (6)$$

After the hyperparameter $\boldsymbol{\gamma}$ is estimated, yielding the estimated covariance matrix $\widehat{\boldsymbol{\Sigma}}_{\boldsymbol{d}}$, a MAP point estimate of $\boldsymbol{d}$ can be computed

$$\widehat{\boldsymbol{d}} = \widehat{\boldsymbol{\Sigma}}_{\boldsymbol{d}}\mathbf{G}^T(\boldsymbol{\Sigma_n} + \mathbf{G}\widehat{\boldsymbol{\Sigma}}_{\boldsymbol{d}}\mathbf{G}^T)^{-1}\boldsymbol{p} \quad (7)$$

with

$$\widehat{\boldsymbol{\Sigma}}_{\boldsymbol{d}} = \sum_i \widehat{\gamma}_i \mathbf{C}_i \quad (8)$$

The choice of covariance set $\mathbf{C} \triangleq \{\mathbf{C}_i : i = 1, \ldots d_{\boldsymbol{\gamma}}\}$ is essential to the solution. A single-component assumption that $\boldsymbol{\Sigma_d}$ is an identity matrix leads to a weighted minimum l_2 solution. More interesting covariance terms include the prior information on the scales and locations of the source activities using a mixture of Gaussian kernels of varying scales and locations, which usually leads to a huge $\mathbf{C}$ (on a side, number of dipoles times number of scales). Since the strength of source activity can be considered spatially continuous, representing the source distribution by multiple Gaussian kernels is insufficient and inefficient. In addition, the choice of scale is usually arbitrarily, although it may significant effect the final solution. Furthermore, the covariance basis of $\mathbf{C}_i$ is usually diagonal, which ignores the correlation between the dipole currents.

III. An Alternative Correlation Model-the SCS Algorithm

Instead of modeling the sources as a mixture of multiple Gaussian kernels, here we propose a correlation-variance model that exploits the fact that one can factor any full-rank covariance matrix into the multiplication of a correlation matrix and the square roots of the diagonal variance matrix as follows:

$$\boldsymbol{\Sigma_d} = \mathbf{V}^{\frac{1}{2}}\mathbf{R}\mathbf{V}^{\frac{1}{2}}, \mathbf{V}(i,i) = \sigma_i^2 \quad (9)$$

The matrix element $\mathbf{R}(i,j)$ is the correlation coefficient between the strengths of the ith and jth dipoles, whose value assumed to be given by a prior estimate. Assuming a local tendency toward synchronization of neural activities at nearby dipoles in the source space, this correlation may be assumed to be exponentially decreasing as the squared distance between dipole locations. A direct definition of the correlation matrix could be

$$\mathbf{R}_{i,j}=\exp(-a\,\|\boldsymbol{r}(i)-\boldsymbol{r}(j)\|), \forall i,j = 1, \ldots, n \quad (10)$$

where $\boldsymbol{r}(i)$ denotes the location of the ith dipole and $\|\boldsymbol{r}(i)-\boldsymbol{r}(j)\|$ is the the Euclidean distance between dipole i and dipole j. However, to guarantee the positive definiteness of the correlation coefficient matrix $\mathbf{R}$, instead of using the definition in (10) we introduce another matrix H with the same dimension of $\mathbf{R}$ such that

$$\mathbf{R} = \mathbf{H}\,\mathbf{H}^{\mathrm{T}}$$

Here, we assume the that the components of $\mathbf{H}$ are given by

$$\mathbf{H}(i,j)=c_i\,(1+\exp(\,a\,\|\boldsymbol{r}(i)-\boldsymbol{r}(j)\|-b\,))^{-1} \quad \forall i,j = 1, \ldots, n \quad (11)$$

$$\mathbf{H}(i,j) = \frac{c_i}{1+\exp\left(a\,\|\,\mathbf{r}(i)-\mathbf{r}(j)\,\|-b\right)} \qquad \forall i,j = 1,\mathrm{L}\ ,n$$

with

$$c_i = \frac{1}{\sqrt{\sum_{i=1}^{n}(1+\exp(a\|\boldsymbol{r}(i)\,\boldsymbol{r}(j)\|-b))^2}} \quad \forall i,j = 1, \ldots, n \quad (12)$$

The parameter b is related to the distance within which the correlation coefficient remains at a relatively high level; a is related to the decay rate of the correlation coefficient beyond that distance; c_i is a scaling factor that makes $\mathbf{R}(i,i)=1$. The values of a and b can either be predefined or learned from the data. After setting proper values for a and b, most entries of $\mathbf{H}$ will be close to zero, i.e. $\mathbf{H}$ will be a sparse matrix. Therefore, the heavy computation load due to the high dimension of $\mathbf{H}$ is greatly reduced. In fact, iteration speed of SCS is faster than SBL.

The major thrust of the *Sparse Compact Smooth* (SCS) algorithm is to learn from the data the variance of the dipole sources $\boldsymbol{\sigma} \triangleq [\sigma_i, \ldots \sigma_n]^T$ and $\boldsymbol{\varepsilon} \triangleq [\varepsilon_i, \ldots \varepsilon_m]^T$, the noise variance under the $\boldsymbol{\gamma}$-MAP framework:

$$(\widehat{\boldsymbol{\sigma}}, \widehat{\boldsymbol{\varepsilon}}) = \arg\min_{\boldsymbol{\sigma},\boldsymbol{\varepsilon}} L\,(\boldsymbol{\sigma}, \boldsymbol{\varepsilon}) \quad (13)$$

with

$$\boldsymbol{L}(\boldsymbol{\sigma}, \boldsymbol{\varepsilon}) = \boldsymbol{p}^T\boldsymbol{\Sigma}_{\boldsymbol{p}}^{-1}\boldsymbol{p} + \log(|\boldsymbol{\Sigma}_{\boldsymbol{p}}|) \quad (14)$$

where $\boldsymbol{\Sigma_p}$ is defined as in (6)

IV. The Optimization of Variance

We implement the *Sparse Compact Smooth (SCS)* algorithm by using an adaptive gradient approach to updating the *a posteriori* estimate of σ_i and ε_i. This is a distinct difference from the way the EM algorithm is used by SBL-based approaches. Here, it avoids the computational difficulty due to the non-diagonal structure of $\boldsymbol{\Sigma_d}$.

It is easy to prove that the point estimate of $\boldsymbol{d}$ in (7) is invariant to multiplication of $(\boldsymbol{\sigma}, \boldsymbol{\varepsilon})$ by a positive scalar (i.e., the point estimate of $\boldsymbol{d}$ is unchanged after $\boldsymbol{\sigma}$ and $\boldsymbol{\varepsilon}$ are both multiplied by the same arbitrary positive factor). However, the cost function in (14) does depend on such a scalar multiplication of $(\boldsymbol{\sigma},\boldsymbol{\varepsilon})$ Exploiting this fact, given $\boldsymbol{\sigma}$ and $\boldsymbol{\varepsilon}$, we find the factor k that minimizes the cost function $\boldsymbol{L}(k\boldsymbol{\sigma},k\boldsymbol{\varepsilon})$.

$$\begin{aligned} k^* &= \arg\min_k \boldsymbol{L}(k\boldsymbol{\sigma}, k\boldsymbol{\varepsilon}) \\ &= \arg\min_k \boldsymbol{p}^T\boldsymbol{\Sigma}_{\boldsymbol{p}}^{-1}\boldsymbol{p}/k+\log(|\boldsymbol{\Sigma}_{\boldsymbol{p}}|)k^m) \\ &= \arg\min_k \boldsymbol{p}^T\boldsymbol{\Sigma}_{\boldsymbol{p}}^{-1}\boldsymbol{p}/k+\log(|\boldsymbol{\Sigma}_{\boldsymbol{p}}|)+m\log(k) \end{aligned} \quad (15)$$

Eq. (15) can be computed analytically,

$$k^* = \boldsymbol{p}^T\boldsymbol{\Sigma}_{\boldsymbol{p}}^{-1}\boldsymbol{p}/m \quad (16)$$

$$\boldsymbol{L}(k^*\boldsymbol{\sigma},k^*\boldsymbol{\varepsilon}) = m+\log(|\boldsymbol{\Sigma}_{\boldsymbol{p}}|)+m\log(\boldsymbol{p}^T\boldsymbol{\Sigma}_{\boldsymbol{p}}^{-1}\boldsymbol{p})-m\log(m) \quad (17)$$

Equation (17) is determined by $\boldsymbol{\sigma}$ and $\boldsymbol{\varepsilon}$ and is invariant to a multiplication of $(\boldsymbol{\sigma}, \boldsymbol{\varepsilon})$ by k (i.e., (17) is constant in value on the ray through the point $(\boldsymbol{\sigma}, \boldsymbol{\varepsilon})$). Therefore, the cost function $\boldsymbol{L}(\mathrm{k}, \varepsilon)$ in (14) can be replaced by

$$\boldsymbol{L}^*(\boldsymbol{\sigma},\boldsymbol{\varepsilon}) = \log(|\boldsymbol{\Sigma}_{\boldsymbol{p}}|)+m\log(\boldsymbol{p}^T\boldsymbol{\Sigma}_{\boldsymbol{p}}^{-1}\boldsymbol{p}) \quad (18)$$

Using (18) as the cost function to be optimized is much more efficient than (14), since a search along the ray through each point ($\boldsymbol{\sigma}$, $\boldsymbol{\varepsilon}$) is avoided. (Effectively we are always at the optimal location on each ray, so the optimization is essentially done over the set of rays.)

To guarantee that the values of σ_i and ε_j are positive, we take σ_i, ε_j to be the exponential of real numbers φ_i and η_j respectively. The optimization is now performed on the vectors $\boldsymbol{\varphi}$ and $\boldsymbol{\eta}$, $\boldsymbol{\varphi} \triangleq [\varphi_1,\ldots,\varphi_n]^T$, $\boldsymbol{\eta} \triangleq [\eta_1,\ldots,\eta_m]^T$.

$$(\hat{\boldsymbol{\varphi}}, \hat{\boldsymbol{\eta}}) = \arg\min_{\boldsymbol{\varphi},\boldsymbol{\eta}} \boldsymbol{L}^*(\exp(\boldsymbol{\varphi}), \exp(\boldsymbol{\eta})) \quad (19)$$

using

$$\exp(\boldsymbol{\varphi}) = [\exp(\varphi_1),\ldots,\exp(\varphi_n)]^T, \exp(\boldsymbol{\eta}) = [\exp(\eta_1),\ldots,\exp(\eta_m)]^T, \quad (20)$$

The gradient of Eq.(19) is

$$\frac{\partial \boldsymbol{L}^*}{\partial \varphi_i} = \left(\mathrm{tr}\left(\boldsymbol{\Sigma}_{\boldsymbol{p}}^{-1}\frac{\partial \boldsymbol{\Sigma}_{\boldsymbol{p}}}{\partial \sigma_i}\right) - m\boldsymbol{p}^T\boldsymbol{\Sigma}_{\boldsymbol{p}}^{-1}\frac{\partial \boldsymbol{\Sigma}_{\boldsymbol{p}}}{\partial \sigma_i}\boldsymbol{\Sigma}_{\boldsymbol{p}}^{-1}\boldsymbol{p}/\boldsymbol{p}^T\boldsymbol{\Sigma}_{\boldsymbol{p}}^{-1}\boldsymbol{p}\right)\exp(\varphi_i),\ \forall i = 1,\ldots,n$$

$$\frac{\partial \boldsymbol{L}^*}{\partial \eta_j} = \left(\mathrm{tr}\left(\boldsymbol{\Sigma}_{\boldsymbol{p}}^{-1}\frac{\partial \boldsymbol{\Sigma}_{\boldsymbol{p}}}{\partial \varepsilon_j}\right) - m\boldsymbol{p}^T\boldsymbol{\Sigma}_{\boldsymbol{p}}^{-1}\frac{\partial \boldsymbol{\Sigma}_{\boldsymbol{p}}}{\partial \varepsilon_j}\boldsymbol{\Sigma}_{\boldsymbol{p}}^{-1}\boldsymbol{p}/\boldsymbol{p}^T\boldsymbol{\Sigma}_{\boldsymbol{p}}^{-1}\boldsymbol{p}\right)\exp(\eta_j),\ \forall j = 1,\ldots,m \quad (21)$$

with

$$\frac{\partial \boldsymbol{\Sigma}_{\boldsymbol{p}}}{\partial \sigma_i} = \boldsymbol{g}_i\boldsymbol{h}_i\mathbf{H}^T\mathbf{V}\mathbf{G} + \mathbf{G}^T\mathbf{V}^T\mathbf{H}\boldsymbol{h}_i^T\boldsymbol{g}_i^T, \forall i = 1,\ldots,n \quad (22)$$

Where

$\boldsymbol{g}_i$ is the ith column vector of $\mathbf{G}$, $\boldsymbol{h}_i$ is the ith row vector of $\mathbf{H}$

$$\frac{\partial \boldsymbol{\Sigma}_{\boldsymbol{p}}}{\partial \varepsilon_j} = \boldsymbol{\delta}_{(i)}\boldsymbol{\delta}_{(i)}{}^T, \forall i = 1,\ldots,m \quad (23)$$

Here $\boldsymbol{\delta}_{(i)}$ is a $m\times 1$ vector such that $\boldsymbol{\delta}_{(i)}[i]=1, \forall i = 1,\ldots,m$ and other elements are zero. The dimensional scaling invariant property of (16) defined in ($\boldsymbol{\sigma}$,$\boldsymbol{\varepsilon}$) is now replaced by the shift-invariant property with respect to ($\boldsymbol{\varphi}$, $\boldsymbol{\eta}$), that is

$$\boldsymbol{L}^*(\exp(\boldsymbol{\varphi}),\exp(\boldsymbol{\eta})) = \boldsymbol{L}^*(\exp(\boldsymbol{\varphi}+c),\exp(\boldsymbol{\eta}+c)) \quad \forall c \in R \quad (24)$$

To speed up the convergence, we further constrain ($\boldsymbol{\varphi}$, $\boldsymbol{\eta}$) to the hyperplane $\boldsymbol{V}$,

$$\boldsymbol{V} = \{(\boldsymbol{\varphi},\boldsymbol{\eta}) \in \mathbf{R}^{m+n} : \sum_{i=1}^{n}\varphi_i + \sum_{j=1}^{m}\eta_j - c = 0 \quad (25)$$

The gradient of $\boldsymbol{L}^*$ projected onto the hyperplane $\boldsymbol{V}$ is

$$\frac{\partial \boldsymbol{L}^*}{\partial(\boldsymbol{\varphi},\boldsymbol{\eta})}|\boldsymbol{V} = \frac{\partial \boldsymbol{L}^*}{\partial(\boldsymbol{\varphi},\boldsymbol{\eta})} - \mathbf{1}\mathbf{1}^T\frac{\partial \boldsymbol{L}^*}{\partial(\boldsymbol{\varphi},\boldsymbol{\eta})} \quad (26)$$

With $\mathbf{1} \triangleq [1,\ldots 1]$, $\mathbf{1} \in \mathbf{R}^{m+n}$. We adopt a Steepest Descent with Adaptive Stepsize (SDAS) [9] algorithm to update $\boldsymbol{\varphi}_k, \boldsymbol{\eta}_k$

$$[\boldsymbol{\varphi}_k^T, \boldsymbol{\eta}_k^T]^T = [\boldsymbol{\varphi}_{k-1}^T, \boldsymbol{\eta}_{k-1}^T]^T + \alpha_k\frac{\partial \boldsymbol{L}^*}{\partial(\boldsymbol{\varphi}_{k-1},\boldsymbol{\eta}_{k-1})}|\boldsymbol{V} \quad (27)$$

$$\alpha_k = |[\boldsymbol{\varphi}_{k-1}^T, \boldsymbol{\eta}_{k-1}^T]^T - [\boldsymbol{\varphi}_{k-2}^T, \boldsymbol{\eta}_{k-2}^T]^T| / \left|\frac{\partial \boldsymbol{L}^*}{\partial(\boldsymbol{\varphi}_{k-1},\boldsymbol{\eta}_{k-1})} - \frac{\partial \boldsymbol{L}^*}{\partial(\boldsymbol{\eta}_{k-2},\boldsymbol{\eta}_{k-2})}\right| \quad (28)$$

V. Evaluation of the Quality of the Solution

Since in the most cases, the actual source activities are not known, and neither are the 'true" models of the source activities, minimizing the cost function in (14) alone cannot guarantee a 'true' solution. In addition, because of the different model bases, solutions from different inverse algorithms may differ. Therefore, aspects of the solutions with physiological meaning independent of the models are particular useful for comparing different algorithms and to avoid overlearning. Here *disf* is of particular interest, where

$$disf(\hat{\boldsymbol{d}}) = \hat{\boldsymbol{d}}^T\boldsymbol{D}\hat{\boldsymbol{d}}/d_{max}{}^2 \quad (29)$$

With

$$\boldsymbol{D}_{i,j} = \|\boldsymbol{r}(i),\boldsymbol{r}(j)\|, \forall i = 1,\ldots,n \quad (30)$$

d_{max} is the largest element of vector $\mathrm{abs}(\hat{\boldsymbol{d}}) \triangleq [|d_1|,\ldots,|d_n|]^T$ (31)

Here *disf* represents the spatial diffusion of the brain activity. A useful inverse solution for a maximally independent source should have low *disf*.

VI. Simulation and Results

A. Simulation results

As an initial test of the performance of SCS, we simulated EEG data using a realistic source space incorporating 78,048 current dipole elements oriented perpendicular to a cortical surface extracted from a human MR head image. A gain (or 'lead field') matrix of source projections to 346 simulated scalp channels was computed using BEM modeling tools in the NFT toolbox [10]. To provide a first test, a pair of gaussian-tapered source-space dipole patches were selected to simulate an EEG source. No noise was added to this simulation. We compared the result of applying SCS with that of the SBL method of Wipf and colleagues [3]. The simulated source is depicted in Fig 1 (left panel). The source distributions reconstructed from the source scalp projection by SBL and SCS are shown in the center and right panels, respectively. SBL gave a more scattered (though also sparse) solution, while SCS converged to a maximally compact and smooth solution highly similar to the simulated source.

To test the robustness of the algorithm in the presence of noise, we simulated spatially correlated noise by projecting white noise in the source space through the lead field matrix and adding the result to the projected simulated source. SNRs used in the simulation were 5 dB and 10 dB. SCS again gave a more compact solution in the 5 dB SNR case.

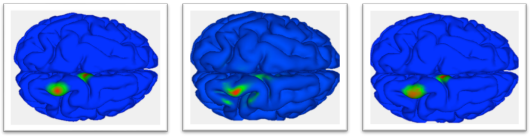

(a) (b) (c)

Fig.1. (a) The EEG source simulation here consisted of two gaussian-tapered patches, a superficial patch on the parietal gyrus and a deeper patch near the longitudinal fissure. Here color is scaled by dipole strength, red representing high strength and green low strength (blue=0). (b) The solution found using SBL and (c) by the proposed SCS algorithm

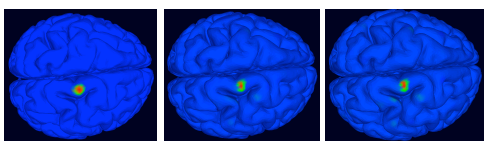

(a) (b) (c)

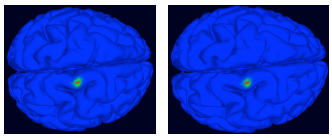

(d) (e)

Fig.1. (a) The simulated EEG source consisted of one gaussian-tapered patch. Solutions found using SBL (b,c) and SCS(d,e) with 10 and 5dB SNR

B. Application to Intracranial EEG Data

Sixteen minutes of 78-channel intracranial EEG data including two brief ictal (seizure) periods recorded by subdural electrodes from an epilepsy patient in Mayo Clinic were used in this study. The brain and the scalp were segmented from the MR images using NFT [10]. 80,130 equivalent current dipoles were generated for subsequent analysis. We applied a recently developed Adaptive Mixture Independent Component Analysis (AMICA) to the data using 5 models, which allowed modeling of non-stationarity in the data source structure [11].

Without loss of generality, we chose the first 30 ICA components from Model 5 for analysis. We applied SCS and SBL inversion. To create a multi-scale cortical patch basis on this brain mesh surface, we selected, for each single-voxel dipole, three conformal, gaussian-tapered cortical patches with geodesic radii of 10 mm, 6 mm, and 3 mm (see [11]). For both algorithms, 30 iterations were used. The convergence criterion was set to $\|\boldsymbol{d}_n - \boldsymbol{d}_{n-1}\|_2 / \|\boldsymbol{d}_{n-1}\| \le 0.001$.

Fig. 2 demonstrates how the solution evolves over iterations. SCS and SBL source estimates at steps 1, 15, and 30 are shown in color scale on the realistic cortical surface estimate. SCS gave a more compact solution than SBL, and this observation was consistent with an analysis of all 30 components analyzed.

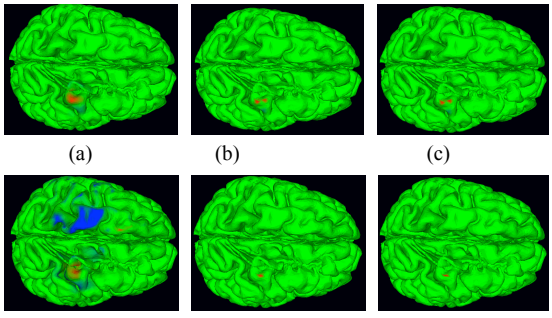

(a) (b) (c)

(d) (e) (f)

Fig.2. (a)-(c) SBL inverse solutions at steps 1, 15, and 30. (d)-(f) SCS inverse solutions at steps 1, 15, and 30. Here, color represents dipole strength, red representing high positive strength and blue, high negative strength (green=0).

The mean *disf* across the 30 components at each iteration is shown in Fig3(a). The *disf* of the SCS solution converges to less than mm^2 while that of SBL solution converges to above $100mm^2$.

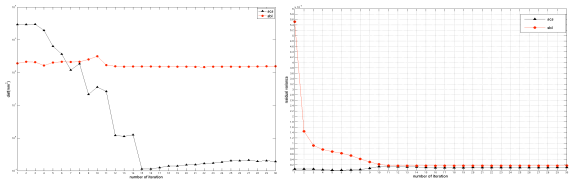

(a) (b)

Fig.3.(a) Mean disf at 30 iterations of SCS (black) and SBL (red) source inversion. (b) Mean normalized residual variance at each SCS (black) and SBL (red) iteration.

The mean normalized residual variance at each iteration steps was depicted in Fig. 3(b) Normalized residual variances of SCS and SBL were both below 2×10^{-6}.

To further investigate the consistency of SCS and SBL inverse solutions, we calculated the distance between the voxel dipoles with highest strength in each solution. Fig. 4 shows that the mean distance between the centers of the SCS and SBL inverse solutions was less than 5 mm.

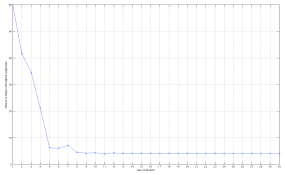

Fig.4. Mean distance between dipoles with highest strength in the SCS and SBL solutions at each iteration.

In these and similar cases, SCS successfully estimates simulated sparse source distributions. SCS may likely be applied as successfully to MEG or EEG source localization problems in cases in which the electromagnetic forward head model is know precisely.

REFERENCES

[1] M. Huang, A. Dale, T. Song, E. Halgren, D. Harrington, I. Podgorny, J. Carnive, S. Lewis, R. Lee, "Vector-based spatial-temporal minimum l1-norm solution for MEG," *NeuroImage* 31(3):1025-1037, 2006.

[2] D. Pascual-Marqui, M. Esslen, K. Kochi, D. Lehmann.,"Functional imaging with low resolution brain electromagnetic tomography (LORETA): a review," *Methods & Findings in Experimental & Clinical Pharmacology*, 24:91-95, 2002.

[3] D. Wipf, S. Nagarajan, " A unified Bayesian framework for MEG/EEG source imaging," *NeuroImage* 44: 947-966, 2009.

[4] K. Friston, L.Harrison, J. Daunizeau, S. Kiebel, C. Phillips, N. Barreto, R. Henson, G. Flandin, J. Mattout, "Multiple sparse priors for the M/EEG inverse problem, " *NeuroImage*, 39(3): 1104-1120, 2008.

[5] D. Wipf. S. Nagarajan, "Iterative Reweighted l_1 and l_2 Methods for Finding Sparse Solutions," *IEEE. J. Selected Topics In Signal Processing*, vol. 4, no. 2, pp.317-329, 2010.

[6] S. Makeig, AJ Bell, T-P Jung, TJ Sejnowski "Independent component analysis of electroencephalographic data," In: *Advances in Neural Information Processing Systems,* vol. 8, D. Touretzky Ed. Cambridge: MIT Press, pp. 8:145-151, 1996.

[7] J. Onton, M. Westerfield, J. Townsend, S. Makeig, "Imaging human EEG brain dynamics using independent component analysis," In: Development Through the Life Cycle, Eds: Ulman Lindenberger and Shu-Chen Li, *Neurosci Behav Reviews* 30:808-822, 2006.

[8] A. Delorme, JA Palmer, J Onton, R Oostenveld, S Makeig, "Independent components of human electroencephalographic data are dipolar," *PLoS One* i7(2):e30135, 2012.

[9] M.N. Vrahatisa, G.S. Androulakisa, J.N. Lambrinosa, G.D. Magoulasb, "A class of gradient unconstrained minimization algorithms with adaptive stepsize," *Journal of Computational and Applied Mathematics*, 114:367-386, 2000.

[10] Z. Akalin Acar, S. Makeig, "Neuroelectromagnetic forward head modeling toolbox", *J Neurosci Meth* , 190:258-270, 2010.

[11] Z. Akalin, J. Palmer, G. Worrell, S. Makeig, "Electrocortical source imaging of intracranial EEG data in epilepsy", in *2011 Proc IEEE Conf Eng Med Biol Soc*., pp. 3909-12.